Journal of the Optical Society of America B
OPTICAL PHYSICS

Hybrid plasmon–phonon polariton bands in graphene–hexagonal boron nitride metamaterials [Invited]

Hodjat Hajian,[1,*] Amir Ghobadi,[1,2] Sina Abedini Dereshgi,[1,2] Bayram Butun,[1] and Ekmel Ozbay[1,2,3,4,5]

[1]NANOTAM-Nanotechnology Research Center, Bilkent University, 06800 Ankara, Turkey
[2]Department of Electrical and Electronics Engineering, Bilkent University, 06800 Ankara, Turkey
[3]Department of Physics, Bilkent University, 06800 Ankara, Turkey
[4]UNAM-Institute of Materials Science and Nanotechnology, Bilkent University, 06800 Ankara, Turkey
[5]e-mail: ozbay@bilkent.edu.tr
*Corresponding author: hodjat.hajian@bilkent.edu.tr

Received 27 February 2017; revised 14 March 2017; accepted 16 March 2017; posted 22 March 2017 (Doc. ID 287650); published 13 April 2017

We theoretically investigate mid-infrared electromagnetic wave propagation in multilayered graphene–hexagonal boron nitride (hBN) metamaterials. Hexagonal boron nitride is a natural hyperbolic material that supports highly dispersive phonon polariton modes in two Reststrahlen bands with different types of hyperbolicity. Due to the hybridization of surface plasmon polaritons of graphene and hyperbolic phonon polaritons of hBN, each isolated unit cell of the graphene–hBN metamaterial supports hybrid plasmon–phonon polaritons (HPPs). Through the investigation of band structure of the metamaterial we find that, due to the coupling between the HPPs supported by each unit cell, the graphene–hBN metamaterial can support HPP bands. The dispersion of these bands can be noticeably modified for different thicknesses of hBN layers, leading to the appearance of bands with considerably flat dispersions. Moreover, analysis of light transmission through the metamaterial reveals that this system is capable of supporting high-k propagating HPPs. This characteristic makes graphene–hBN metamaterials very promising candidates for the modification of the spontaneous emission of a quantum emitter, hyperlensing, negative refraction, and waveguiding.

OCIS codes: (240.6680) Surface plasmons; (240.5420) Polaritons; (160.3918) Metamaterials.

https://doi.org/10.1364/JOSAB.34.000D29

1. INTRODUCTION

Heterostructures composed of graphene and hexagonal boron nitride (hBN) have recently attracted a great deal of attention due to their unusual electronic band structure, which is sensitive to the crystallographic alignment between graphene and hBN [1–3] and also because of their optical properties [4–6]. hBN is a natural hyperbolic material, for which the dielectric constants are the same in the basal plane ($\epsilon_t \equiv \epsilon_x = \epsilon_y$) but have opposite signs ($\epsilon_t \epsilon_z < 0$) in the normal one ($\epsilon_z$) in the mid-infrared (mid-IR) region. Owing to this property, finite-thickness slabs of hBN act as multimode waveguides for the propagation of hyperbolic phonon polariton collective modes that originate from the coupling between photons and electric dipoles in phonons [7–9]. On the other hand, graphene has been demonstrated to be a good candidate to support surface plasmon polaritons for tunable plasmonics in the mid-infrared and terahertz ranges, owing to the possibility of electrostatic doping and its ability to produce higher confinement and lower losses compared to the noble metals [10–16]. Since both graphene plasmons and hBN phonons reside in the mid-IR, the optical properties of graphene–hBN heterostructures would allow one to marry the advantage of their constituents: electrical tunability in the former and high quality factor of the latter. Therefore, recently it has been investigated theoretically [4] and verified experimentally [5,6,9] that, due to the hybridization of surface plasmon polaritons in graphene with the hyperbolic phonon polaritons of a thin film of hBN, the hyperbolic polaritons can be effectively modulated in a van der Waals heterostructure composed of a monolayer of graphene on hBN. Consequently, the eigenmodes of the graphene–hBN metastructure are hybrid plasmon–phonon polaritons (HPPs) [9]. The HPPs in graphene–hBN suffer little from ohmic losses, making their propagation length 1.5–2.0 times greater than that of hyperbolic phonon polaritons in hBN [5].

Similar to the natural hyperbolic materials, e.g., hBN, hyperbolic metamaterials (HMMs) [13–18] can also support modes with infinitely large wave vectors (high-k modes). In HMMs, the opposite signs of the dielectric permittivity components in two orthogonal directions lead to the hyperbolic

dispersion of TM-polarized propagating waves. The high-k modes are evanescent in isotropic media but become propagating in indefinite/hyperbolic ones. As a result, the photonic density of states becomes unbounded in these systems, giving rise to a variety of potential applications, such as hyperlensing [19], engineering of spontaneous emission, broadband Purcell effect, subwavelength imaging, negative refraction, and waveguiding [20–22]. In fact, high-k propagating waves in HMMs are volume or Bloch plasmon polaritons. The volume plasmon polariton bands in a metal-based HMM are formed by coupling of short-range surface plasmon polariton excitations in the individual metal layers [23]. Similarly, in a graphene–dielectric metamaterial, the same mechanism also leads to the formation of the Bloch propagating bands [24]. Depending on the desired range of frequency, the multilayered realization of HMMs may consist of alternating subwavelength layers of dielectric and semiconductor/plasmonic materials, such as Au, Ag, AZO, ITO, and graphene [25–29]. Recently, it has also been reported that it is possible to combine the properties of hyperbolic metamaterials and those of photonic crystals [30] in a new class of artificial structures called hypercrystals [31]. Hypercrystals can be made of the periodic arrangements of metal and a hyperbolic medium, dielectric and a hyperbolic medium, or two different hyperbolic media. It is noteworthy that the hyperbolic medium can either be a natural material with hyperbolic dispersion, such as bismuth [32], or an artificial one, i.e., HMM [31]. The photonic hypercrystals have also perceptible potential applications, such as guiding [31] and the broadband enhancement of spontaneous emission [33]. Moreover, the multilayered structure of the graphene–hBN subwavelength stack can also be considered as a hypercrystal, as far as the effective medium theory (EMT) does not break down. As a result, considering a finite thickness for multilayered graphene sheets in the graphene–hBN hypercrystal and using the EMT approach, it has been demonstrated that it is possible to obtain negative refraction [34] and broadband absorption [35] by this system in the mid-IR region. To the best of our knowledge, the band structure of multilayered graphene–hBN metamaterials (GhMMs), which can act as either hypercrystal or metamaterial, and the appearance of high-k modes in their band structure have not yet been investigated.

In the present paper, in Section 2, considering graphene as a two-dimensional sheet with the optical conductivity of σ_g, first we obtain TE and TM Bloch dispersion relations of GhMMs. Then, using the transfer matrix method (TMM), the analytical transmission relation of this system will be derived. Finally, in Section 3, we will compare the numerical results of the band structure calculations with the transmission of the GhMMs and investigate the high-k HPPs supported by these structures. It should be noticed that since the HPs of a thin film of hBN are highly dispersive for large values of wavenumbers, for which the EMT approximation may break down, we investigate the multilayered graphene–hBN structures using exact analytical dispersion relations. Therefore, we call these structures *metamaterials*, not *hypercrystals*.

2. MATH AND EQUATIONS

As depicted in Fig. 1(a), we suppose that each unit cell of the GhMM is composed of a parallel-plate waveguide of graphene separated and bounded with hBN thin films of width t. We refer

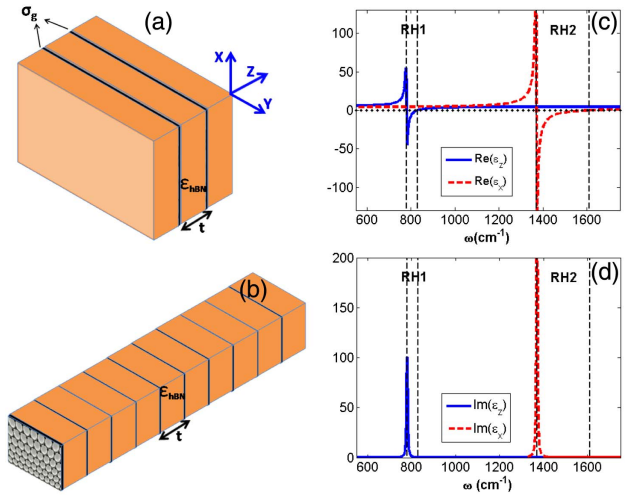

Fig. 1. Panels (a) and (b) respectively illustrate an isolated unit cell of the GhMM, which is referred to as hGhGh and the GhMM under our consideration in this paper. Panels (c) and (d) show the real and imaginary values of ϵ_x and ϵ_z of hBN, respectively. The vertical dashed lines in these panels illustrate the boundary of the Reststrahlen bands noted as RH1 and RH2 in these panels.

to this unit cell as a hBN/graphene/hBN/graphene/hBN metastructure or briefly hGhGh. Accordingly, the schematic of the graphene–hBN metamaterial is also depicted in Fig. 1(b).

TM and TE boundary conditions for a single graphene sheet as a 2D layer with surface conductivity of σ_g [25] placed in $z = 0$ and bounded with an isotropic medium of ϵ_A and hBN as a uniaxially anisotropic medium with permittivity tensor $\epsilon_{\rm hBN} = {\rm diag}(\epsilon_t, \epsilon_t, \epsilon_z)$ may be expressed as

$$E_x|_{z=0^+} = E_x|_{z=0^-}, \tag{1a}$$

$$\frac{\epsilon_t}{k_{h,\rm TM}^2}\frac{dE_x}{dz}\bigg|_{z=0^+} - \frac{\epsilon_A}{k_A^2}\frac{dE_x}{dz}\bigg|_{z=0^-} = \alpha E_x|_{z=0}, \tag{1b}$$

and

$$E_y|_{z=0^+} = E_y|_{z=0^-}, \tag{2a}$$

$$\frac{dE_y}{dz}\bigg|_{z=0^+} - \frac{dE_y}{dz}\bigg|_{z=0^-} = \beta_0^2 \alpha E_y|_{z=0}, \tag{2b}$$

respectively. Here, $\alpha = \sigma_g/i\omega\epsilon_0$, $k_{h,\rm TM} = \sqrt{\epsilon_t(\epsilon_z\beta_0^2 - \beta^2)/\epsilon_z}$, $k_A = \sqrt{\epsilon_A\beta_0^2 - \beta^2}$, $\beta_0 = \omega/c$, $\beta = k_t$, and

$$\epsilon_m = \epsilon_{\infty,m} \times \left[1 + \frac{\omega_{{\rm LO},m}^2 - \omega_{{\rm TO},m}^2}{\omega_{{\rm TO},m}^2 - \omega^2 - i\omega\Gamma_m}\right], \qquad m = t, z. \tag{3}$$

Now, combining the methods used in Refs. [36,37] and applying the TM boundary conditions [Eq. (1)], the Bloch dispersion relation of the GhMM for TM polarization is given by

$$\cos(K_B t) = \cos(k_{h,\rm TM} t) + \frac{\alpha k_{h,\rm TM}}{2\epsilon_t}\sin(k_{h,\rm TM} t), \tag{4}$$

where K_B is the Bloch wavenumber. Moreover, the corresponding dispersion relation for TE polarization is obtained as

$$\cos(K_B t) = \cos(k_{h,\mathrm{TE}} t) + \frac{\alpha\beta_0^2}{2k_{h,\mathrm{TE}}} \sin(k_{h,\mathrm{TE}} t), \tag{5}$$

where $k_{h,\mathrm{TE}} = \sqrt{\epsilon_t \beta_0^2 - \beta^2}$. Furthermore, in order to be able to examine the origin of the bands that appear in the TM-projected band structure of the GhMMs, we also would like to obtain a TM dispersion relation of guided HPP modes supported by one isolated unit cell of the structure, i.e., hGhGh metastructure [see Fig. 1(a)]. To this aim, we consider H_y as

$$H_y(z) = \begin{Bmatrix} H_1 e^{-ik_{h,\mathrm{TM}}(z-t/2)} & z > t/2 \\ H_2 \sin(ik_{h,\mathrm{TM}} z)[\mathrm{odd}] & -t/2 \le z \le t/2 \\ H_2 \cos(ik_{h,\mathrm{TM}} z)[\mathrm{even}] & -t/2 \le z \le t/2 \\ H_3 e^{ik_{h,\mathrm{TM}}(z+t/2)} & z < -t/2 \end{Bmatrix}. \tag{6}$$

Then, by applying the TM boundary conditions in Eq. (6), we arrive at the dispersion relation of the guided modes supported by the hGhGh unit cell as

$$\tan(k_{h,\mathrm{TM}} t/2) = \begin{Bmatrix} \eta, & H_y \text{ odd} \\ 1/\eta, & H_y \text{ even} \end{Bmatrix}, \tag{7}$$

where $\eta = i + \alpha k_{h,\mathrm{TM}}/\epsilon_t$.

It is also worth investigating the transmission spectrum of the graphene–hBN metamaterial to be able to get more insight into how transmissive the modes that appeared in the projected band structure of the metamaterial are. Using the TMM approach, we consider an N-layer graphene–hBN metamaterial that is bounded with isotropic medium with ϵ_A. The first layer of the metamaterial is considered to be a single graphene sheet placed at $z = 0$. Applying the boundary conditions for TM polarizations [Eq. (1)] on

$$H_y(z) = \begin{Bmatrix} H_i e^{ik_A z} + H_r e^{-ik_A z}, & z < 0 \\ H_{n1} e^{ik_{h,\mathrm{TM}}[z-(n-1)t]} + H_{n2} e^{-ik_{h,\mathrm{TM}}[z-(n-1)t]}, & (n-1)t < z < nt \\ H_t e^{ik_A(z-nt)}, & z > nt \end{Bmatrix}, \tag{8}$$

where $n = 1, 2, 3, \ldots, N$, the analytical relation for transmission of light through the metamaterial can be expressed as

$$T = |H_t/H_i|^2 = |1/M_{11}|^2, \tag{9}$$

where

$$M = \begin{bmatrix} M_{11} \\ M_{12} \end{bmatrix} = m_{A1}^{-1} (m_1 m_2^{-1})^N m_{A2}. \tag{10}$$

Here, for TM polarization,

$$m_{A1} = \begin{bmatrix} ik_A/\epsilon_A & -ik_A/\epsilon_A \\ 1 - i\alpha k_A/\epsilon_A & 1 + i\alpha k_A/\epsilon_A \end{bmatrix}, \tag{11a}$$

$$m_{A2} = \begin{bmatrix} ik_A/\epsilon_A \\ 1 \end{bmatrix}, \tag{11b}$$

and

$$m_1 = \begin{bmatrix} ik_{h,\mathrm{TM}}/\epsilon_t & -ik_{h,\mathrm{TM}}/\epsilon_t \\ 1 & 1 \end{bmatrix}, \tag{12a}$$

$$m_2 = \begin{bmatrix} ik_{h,\mathrm{TM}} e^{ik_{h,\mathrm{TM}} t}/\epsilon_t & -ik_{h,\mathrm{TM}} e^{-ik_{h,\mathrm{TM}} t}/\epsilon_t \\ (1 - i\alpha k_{h,\mathrm{TM}}/\epsilon_t) e^{ik_{h,\mathrm{TM}} t} & (1 + i\alpha k_{h,\mathrm{TM}}/\epsilon_t) e^{-ik_{h,\mathrm{TM}} t} \end{bmatrix}. \tag{12b}$$

For TE polarization, by applying the appropriate boundary conditions on

$$E_y(z) = \begin{Bmatrix} E_i e^{ik_A z} + E_r e^{-ik_A z}, & z < 0 \\ E_{n1} e^{ik_{h,\mathrm{TE}}[z-(n-1)t]} + E_{n2} e^{-ik_{h,\mathrm{TE}}[z-(n-1)t]}, & (n-1)t < z < nt \\ E_t e^{ik_A(z-nt)}, & z > nt \end{Bmatrix}, \tag{13}$$

the transmission relation can be obtained similar to Eqs. (9) and (10), while

$$m_{A1} = \begin{bmatrix} 1 & 1 \\ ik_A + \alpha\beta_0^2 & -ik_A + \alpha\beta_0^2 \end{bmatrix}, \tag{14a}$$

$$m_{A2} = \begin{bmatrix} 1 \\ ik_A \end{bmatrix}, \tag{14b}$$

and

$$m_1 = \begin{bmatrix} 1 & 1 \\ ik_{h,\mathrm{TE}} & -ik_{h,\mathrm{TE}} \end{bmatrix}, \tag{15a}$$

$$m_2 = \begin{bmatrix} e^{ik_{h,\mathrm{TE}} t} & e^{-ik_{h,\mathrm{TE}} t} \\ (ik_{h,\mathrm{TE}} + \alpha\beta_0^2) e^{ik_{h,\mathrm{TE}} t} & (-ik_{h,\mathrm{TE}} + \alpha\beta_0^2) e^{-ik_{h,\mathrm{TE}} t} \end{bmatrix}. \tag{15b}$$

3. RESULTS AND DISCUSSION

In this section, first we investigate the band structure of the graphene–hBN multilayer metamaterial, which is schematically shown in Fig. 1(b), for different values of hBN thickness (t). Here, we chose $T = 300$ K, $\mu = 0.2$ eV, and $\tau = 0.2$ ps in our calculations for the optical conductivity of graphene, unless otherwise stated. Furthermore, following Refs. [6,8], the parameters for the calculation of hBN permittivity in Eq. (2) are taken as $\epsilon_{\infty,x} = 2.95$, $\epsilon_{\infty,z} = 4.87$, $\omega_{\mathrm{LO},x} = 1610\ \mathrm{cm}^{-1}$, $\omega_{\mathrm{TO},x} = 1370\ \mathrm{cm}^{-1}$, $\omega_{\mathrm{LO},z} = 830\ \mathrm{cm}^{-1}$, $\omega_{\mathrm{TO},z} = 780\ \mathrm{cm}^{-1}$, $\Gamma_x = 4\ \mathrm{cm}^{-1}$, and $\Gamma_z = 5\ \mathrm{cm}^{-1}$. In addition, in the calculations of transmission, we take ϵ_A as 1. Normal incidence ($\beta = 0$) band structures of the GhMM for different periodicities are illustrated in Fig. 2. These results are represented for both lossy cases and lossless ones; for the latter, $\mathrm{Im}(\sigma_g)$ and $\mathrm{Re}(\epsilon_{\mathrm{hBN}})$ are taken into account. Therefore, it is possible to apply the $|\cos(K_B t)| < 1$ condition on the answers obtained from Eq. (1) to be able to realize the propagating and forbidden Bloch modes of the metamaterials for the lossless cases [Figs. 2(a), 2(c), and 2(e)].

As seen in Figs. 2(c) and 2(d), for normal incidence, the GhMMs do not support a propagating mode in the $\omega_{\mathrm{TO},x} < \omega < \omega_{\text{upper edge}}$ region, for which $\omega_{\text{upper edge}}$ shifts toward $\omega_{\mathrm{LO},x}$ for large enough hBN thicknesses ($t \ge 100$ nm). In the mentioned region, the RH2 band, Eq. (1) supports no answer [$\mathrm{Im}(K_B) \neq 0$], while for the propagating modes, $\mathrm{Im}(K_B) = 0$. In contrast to these figures, as long as the thickness of hBN layers is taken small enough ($t \le 10$ nm), the propagating modes of the metamaterial are supported within a limited region in $1070\ \mathrm{cm}^{-1} < \omega < \omega_{\mathrm{TO},x}$ for normal incidence. The presence of flat bands at $\omega_{\mathrm{TO},x}$ in the band structure of the metamaterial for normal incidence is another point that should be emphasized. As seen in Fig. 2, dispersion of these flat bands approaches $\omega_{\mathrm{TO},x}$ for $K_B t/\pi \to 1$, which resembles the

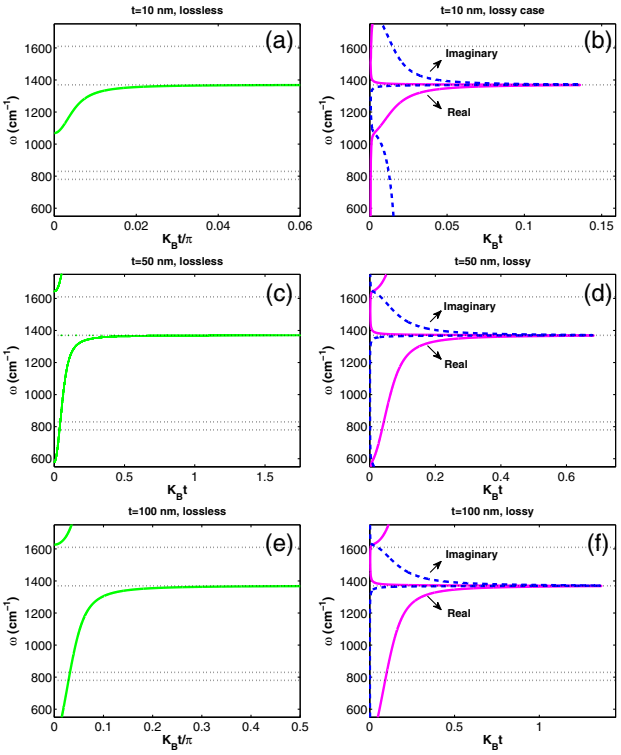

Fig. 2. Panels (a) and (b) respectively represent the band structure of graphene–hBN metamaterial for lossless and lossy cases with $t = 10$ nm. In accordance with panels (a) and (b), panels (c), (d) and (e), (f) show similar results for $t = 50$ nm and $t = 100$ nm GhMMs, respectively.

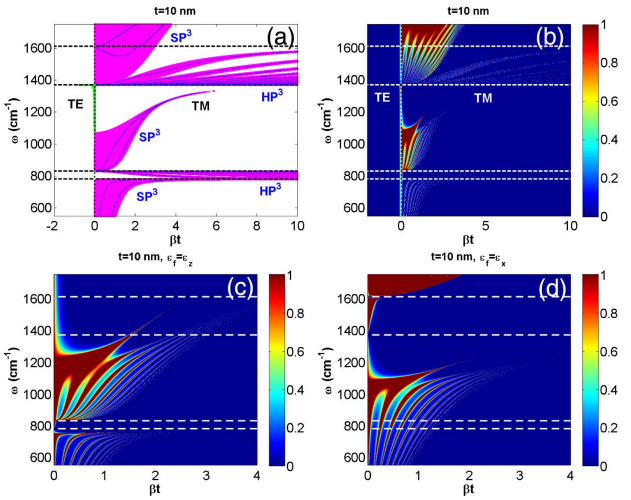

Fig. 3. Panels (a) and (b) respectively illustrate the projected band structure of GhMM with $t = 10$ nm and the transmission of light passing through this system considering $N = 10$ for both TE and TM polarizations; N shows the number of hBN layers taken in the calculations. The solid-blue curves in panel (a) show SP^3 and HP^3 modes supported by an isolated hGhGh unit cell, for which the graphene layers are separated by a 10 nm thin film of hBN. Similar to panel (b), TM light transmission for fictitious metamaterials with $\epsilon_f = \epsilon_z$ and $\epsilon_f = \epsilon_x$ are represented in panels (c) and (d), respectively. Notice that the boundaries of the RH bands, in which hBN has a hyperbolic optical response, are determined with the dashed horizontal lines.

dispersion of the modes supported by a lossless isotropic polaritonic bulk material. Similar to the ones supported by polaritonic photonic crystals [38,39], the appearance of the flat bands in the band structure of the GhMMs is directly due to the coupling of HPPs supported by hGhGh unit cells in the structure. More investigations on the typical band structure ($\omega - K_B$) of the system reveal that, for the nonzero values of β, these flat bands are mostly limited in the first and the second RH bands for TM polarizations, while for TE polarizations they are not supported. For the lossy case, for which the complex values of ϵ_{hBN} and σ_g are taken into account, the normal incidence band structures of the metamaterial for different thicknesses are illustrated in Figs. 2(b), 2(d), and 2(f). In this case, since K_B is complex, it is not possible to apply the $|\cos(K_B t)| < 1$ condition on the answers to separate modes with the zero and nonzero values of $\mathrm{Im}(K_B)$. Consequently, for the mentioned panels of Fig. 2, we illustrate the results by considering both the real and imaginary values of K_B. Similar to the lossless cases, $\mathrm{Im}(K_B)$ of the propagating modes of the metamaterials have very small values [note that $\mathrm{Im}(K_B t/\pi)$ of the propagating modes is zero and of the order of 10^{-4} for the lossless and lossy cases, respectively]. As expected, for nonpropagating modes $\mathrm{Im}(K_B) \gg \mathrm{Re}(K_B)$, when the values of $\mathrm{Im}(K_B)$ and $\mathrm{Re}(K_B)$ are comparable, low-propagating modes are supported by the system. Moreover, the modes with $\mathrm{Im}(K_B) \ll \mathrm{Re}(K_B)$ can propagate through the metamaterial with high transmission values. Furthermore, in contrast to the band structure of the lossless cases, it can be seen in Figs. 2(b), 2(d), and 2(f) that for the lossy system the propagating band approaches a maximum, finite value of $\mathrm{Re}(K_B t/\pi)$ at $\omega_{\mathrm{TO},x}$ and then changes its slope toward larger frequencies. Since there are fair agreements between the typical band structures of the lossless and lossy cases, hereinafter we investigate the projected band structure and transmission of the propagating modes of GhMMs neglecting the losses in the metamaterial.

In agreement with Fig. 2(a), the projected band structure of the GhMM for $t = 10$ nm is illustrated in Fig. 3(a) for both TM and TE polarizations. In this figure, pink (green) and white regions represent the allowed and forbidden bands of the metamaterial for TM (TE) polarizations. Moreover, the dashed lines distinguish the boundaries of the RH1 and RH2 bands in which a film of hBN supports hyperbolic phonon polaritons of type I and II, respectively. As seen from the TE band structure, the propagating modes are supported in a very limited region outside of the RH bands within $1064 < \omega(\mathrm{cm}^{-1}) < 1370$. On the other hand, for TM polarization, because of the coupling between the supported HPPs by each unit cell of the metamaterial, the band structure is drastically different than that of TE polarization. To be able to gain more insight into the origin of the propagating bands (allowed bands) of the structure, the dispersion of the guided HPPs supported by one isolated unit cell of the metamaterial, i.e., hGhGh metastructure, is also illustrated by solid-blue curves in Fig. 3(a). Following Ref. [5], we call these hybrid modes SP^3 and HP^3. Let us consider the surface plasmon polaritons of a parallel-plate waveguide of graphene and hyperbolic phonon polaritons of a thin film of hBN as SP^2 [4,5,40,41] and HP^2 [4,5] modes, respectively. Therefore, the combination of SP^2 and HP^2 waves in each hGhGh unit cell

leads to the appearance of hyperbolic plasmon–phonon polaritons, the HP^3 modes. Following the terminology established in Ref. [5], SP^3 modes are surface plasmon–phonon polaritons of each hGhGh unit cell that are the collective modes that exist outside the hBN hyperbolic bands, i.e., RH bands. From Fig. 3(a), it is clearly observed that there is an excellent agreement between the band structure of the GhMM and the dispersion trends of the HP^3 and SP^3 modes of the hGhGh unit cell. Consequently, we classify the propagating bands of the graphene–hBN metamaterial in the mid-IR region to the following five bands: three SP^3 and two HP^3 bands. With this appellation, it is very straightforward to understand that the SP^3 bands of the metamaterial appear due to the coupling between the corresponding modes of the hGhGh unit cells. The same physics also stands behind the creation of HP^3 hyperbolic bands that are supported in the RH regions. It is noteworthy to highlight this point that due to the same coupling mechanism, metal-based [23] and graphene-based [24,28,42] metamaterials are also capable of supporting such propagating bands. At the $k_h t \ll 1$ condition, for which the effective medium approximation is valid, neither the phase nor the amplitude of a propagating wave varies significantly across the thickness of any layer in the metamaterial. This condition is called the "subwavelength condition" for HMMs [23]. It should be pointed out that in conventional media the subwavelength condition can simply be $t/\lambda \ll 1$ due to the elliptical dispersion relation, which restricts the range of possible β values. In hyperbolic metamaterials, the "subwavelength condition" breaks down for some large β no matter how thin the layers are. According to Fig. 3(a), the dispersion characteristics of SP^3 and HP^3 bands of the structure under our consideration in this paper are mostly noticeable in the regions in which the subwavelength condition breaks down, i.e., in $\beta t > 1$ regions. Consequently, as also mentioned before, in this paper we generally call the graphene–hBN multilayer structure "*metamaterial*" instead of "*hypercrystal*" [31,34]. Another point regarding Fig. 3(a) is the presence of very flat HP^3 (in the RH1 band) and SP^3 bands (around $\omega_{TO,z}$). This characteristic makes the GhMM with $t = 10$ nm a very appropriate candidate for slow light applications within 700 $cm^{-1} < \omega < \omega_{LO,z}$.

It should be noted that the projected band structure of the metamaterial has been illustrated using Eqs. (4) and (5). These equations were derived based on the Bloch theorem with the consideration of an infinite number of the periods in the calculations. In order to be able to obtain practical insight into the minimum number of periods that need to be used in the fabrication of the metamaterial, by taking 10 periods in the calculations we investigated the transmission of light passing through the system for both TE and TM polarizations. The corresponding result is illustrated in Fig. 3(b). By comparing Figs. 3(a) and 3(b), it is seen that there is a fair agreement between the allowed and forbidden bands represented in the projected band structure with the propagating and blocked modes shown in the transmission plot. More investigations reveal that by increasing the number of the periods in the calculations, it is possible to reach a better agreement between the projected band structure and transmission results. From Fig. 3(b), it is observed that some modes with $\beta t < 3$, $\omega_{LO,z} < \omega <$ 1200 cm^{-1}, and $\omega > \omega_{TO,x}$ can propagate inside the metamaterial with high transmission. These waves are, in fact, the high-k propagating HPPs supported by the metamaterial. As a result, because of their resemblance to the volume plasmon polaritons supported by metallic hyperbolic metamaterial [20], they can be considered as volume hybrid plasmon–phonon polaritons supported by the GhMM. In an effort to uncover the impact of the hyperbolic phonons of hBN thin films on the transmission of light passing through the metamaterial, concurrent calculations are performed for fictitious isotropic materials with permittivity (ϵ_f) equal to ϵ_z [Fig. 3(c)] and ϵ_t [Fig. 3(d)] of hBN. It is seen from these panels that (i) the propagating modes supported by the isotropic cases are not supported for high-k values; they are mostly low-k propagating modes ($\beta t < 1$), (ii) for $\epsilon_t = \epsilon_z$, the low-k modes, which possess the characteristics of plasmon polaritons, are supported outside of the RH regions, (iii) in the $\epsilon_t = \epsilon_x$ case, the low-k modes hold the characteristics of phonon polaritons and are limitedly supported in the RH regions.

For $t = 50$ nm, the projected band structure of the GhMM together with the dispersion of HPPs of the isolated hGhGh unit cell are shown in Fig. 4(a). From this figure, it is clearly observed that increasing the thickness of the hBN layers from 10 to 50 nm causes the SP^3 and HP^3 modes of hGhGh to be supported at larger wavenumbers. This change leads to pushing the SP^3 and HP^3 bands of the metamaterial to larger wavenumbers than that of the $t = 10$ nm case, accordingly. By comparing the TM band structure represented in Fig. 4(a) with the one illustrated in Fig. 3(a) it is understood that for $t = 50$ nm, the widths of SP^3 bands are considerably decreased, while the HP^3 band widths are noticeably increased. In addition, in this case flat SP^3 bands around $\omega_{LO,x}$ can be supported for small values of β, while, as mentioned before, these flat bands are supported by the $t = 10$ nm GhMM around $\omega_{TO,z}$ for large values of β. In agreement with Fig. 4(a), the transmission of the propagating high-k HPPs are illustrated in Fig. 4(b). It is clear from this figure that the GhMM with $t = 50$ nm is more capable of supporting high-k propagating HP^3 and SP^3 modes for $\omega > \omega_{TO,x}$. In contrast, for this structure, low-k propagating HPPs can be supported for $\omega < \omega_{TO,z}$ and $\omega_{TO,x} < \omega < 1650$ cm^{-1}.

The projected band structure of the metamaterial for $t =$ 100 nm [Fig. 5(a)] shows that the HPP bands are mostly supported in the RH regions in this case. Moreover, SP^3 bands with an almost flat dispersion can also be supported in a very narrow region in $\omega_{LO,x} < \omega < 1620$ cm^{-1} for a broad range

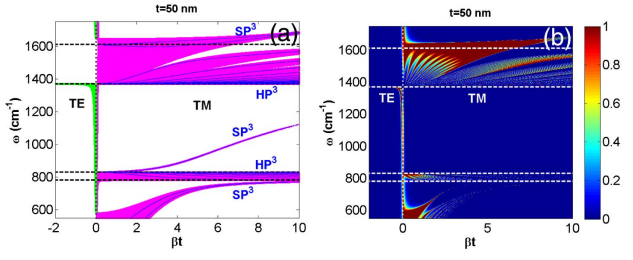

Fig. 4. Panels (a) and (b) respectively show the projected band structure of GhMM with $t = 50$ nm and light transmission through this system for both TE and TM polarizations for $N = 10$. Solid-blue curves in panel (a) represent SP^3 and HP^3 modes of an isolated HGHGH unit cell with $t = 50$ nm. Moreover, horizontal dashed-black lines in panels (a) and (b) highlight the boundaries of the RH bands of hBN.

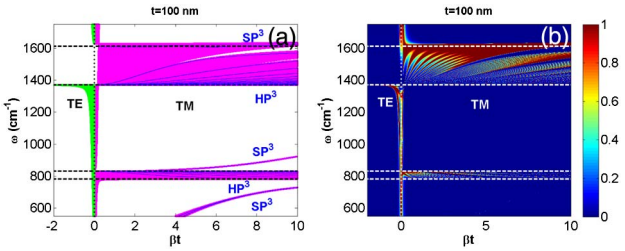

Fig. 5. Similar to Fig. 4, but panels (a) and (b) of this figure are illustrated for $t = 100$ nm.

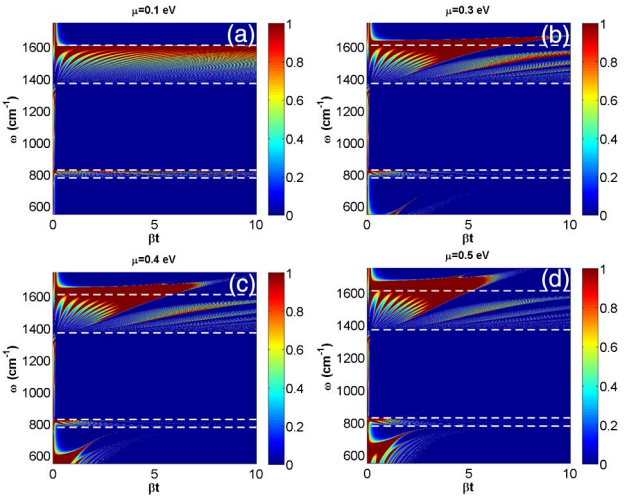

Fig. 6. Panels (a), (b), (c), and (d) represent TM light transmission through the GhMM with $t = 100$ nm for $\mu = 0.1$ eV, $\mu = 0.3$ eV, $\mu = 0.4$ eV, and $\mu = 0.5$ eV, respectively. Notice that the case of $\mu = 0.2$ eV is already presented in Fig. 5(b). It should be noted that these results are obtained for $N = 10$.

of β. In accordance with the projected band structure, considering 10 layers of hBN in the calculations, Fig. 5(b) proves that for $t = 100$ nm more high-k propagating modes that mostly possess HP^3 characteristics can be supported by GHMM at $\omega > \omega_{TO,x}$, compared with the $t = 50$ nm and $t = 10$ nm cases.

The tunability of the low- and high-k propagating HPP modes of the GhMM through the tuning of the chemical potential of graphene is the last point about the high-k propagating HPPs that we would like to highlight. As is seen in Figs. 6(a)–6(d), by adjusting μ it is possible to considerably amend the type of HPP bands from HP^3 to SP^3 and vice versa. This characteristic makes GhMMs highly capable of having potential applications in tunable plasmonic/phononic devices.

4. CONCLUSION

We have theoretically examined the light propagation through a multilayered graphene–hBN metamaterial for both TE and TM polarizations. Each unit cell of the metamaterial supports hybrid plasmon–phonon polaritons for TM polarization. It has been found that due to the coupling between the HPPs of the unit cells, HPP bands appeared in the projected band structure of the GhMMs. These bands have considerably flat dispersions in some frequency regions that make this system very useful for slow light applications. We have classified the HPP bands to HP^3 and SP^3 ones. The HP^3 bands, which are located in the Reststrahlen regions of hBN, are formed by mixing the surface plasmon polaritons of graphene and hyperbolic phonons of hBN, while the SP^3 bands, existing outside of the hBN RH regions, possess the characteristics of typical surface plasmon polaritons of graphene. Moreover, by the investigation of light transmission through the graphene–hBN metamaterials we have found that the HP^3 and SP^3 bands are in fact high-k propagating HPPs and their type and propagation within the metamaterial can be considerably modified by the thickness of hBN and the chemical potential of graphene layers. As a result, this characteristic makes the GhMMs particularly promising for control over radiation of a quantum emitter, hyperlensing, negative refraction, and waveguiding.

Funding. Türkiye Bilimsel ve Teknolojik Araştirma Kurumu (TÜBITAK) (113E331, 114E374); DPT-HAMIT; NATO-SET (193); Turkish Academy of Sciences (TÜBA).

Acknowledgment. H. H. would also like to thank T. Low and A. Nemilentsau for useful discussions.

REFERENCES

1. C. R. Dean, A. F. Young, I. Meric, C. Lee, L. Wang, S. Sorgenfrei, K. Watanabe, T. Taniguchi, P. Kim, K. L. Shepard, and J. Hone, "Boron nitride substrates for high-quality graphene electronics," Nat. Nanotechnol. **5**, 722–726 (2010).
2. A. K. Geim and I. V. Grigorieva, "Van der Waals heterostructures," Nature **499**, 419–425 (2013).
3. M. Yankowitz, J. Xue, D. Cormode, J. D. Sanchez-Yamagishi, K. Watanabe, T. Taniguchi, P. Jarillo-Herrero, P. Jacquod, and B. J. LeRoy, "Emergence of superlattice Dirac points in graphene on hexagonal boron nitride," Nat. Phys. **8**, 382–386 (2012).
4. A. Kumar, T. Low, K. H. Fung, P. Avouris, and N. X. Fang, "Tunable light–matter interaction and the role of hyperbolicity in graphene–hBN system," Nano Lett. **15**, 3172–3180 (2015).
5. S. Dai, Q. Ma, M. K. Liu, T. Andersen, Z. Fei, M. D. Goldflam, M. Wagner, K. Watanabe, T. Taniguchi, M. Thiemens, F. Keilmann, G. C. A. M. Janssen, S.-E. Zhu, P. Jarillo-Herrero, M. M. Fogler, and D. N. Basov, "Graphene on hexagonal boron nitride as a tunable hyperbolic metamaterial," Nat. Nanotechnol. **10**, 682–686 (2015).
6. A. Woessner, M. B. Lundeberg, Y. Gao, A. Principi, P. Alonso-González, M. Carrega, K. Watanabe, T. Taniguchi, G. Vignale, M. Polini, J. Hone, R. Hillenbrand, and F. H. L. Koppens, "Highly confined low-loss plasmons in graphene–boron nitride heterostructures," Nat. Mater. **14**, 421–425 (2015).
7. S. Dai, Z. Fei, Q. Ma, A. S. Rodin, M. Wagner, A. S. McLeod, M. K. Liu, W. Gannett, W. Regan, K. Watanabe, T. Taniguchi, M. Thiemens, G. Dominguez, A. H. Castro Neto, A. Zettl, F. Keilmann, P. Jarillo-Herrero, M. M. Fogler, and D. N. Basov, "Tunable phonon polaritons in atomically thin van der Waals crystals of boron nitride," Science **343**, 1125–1129 (2014).
8. J. D. Caldwell, A. V. Kretinin, Y. Chen, V. Giannini, M. M. Fogler, Y. Francescato, C. T. Ellis, J. G. Tischler, C. R. Woods, A. J. Giles, M. Hong, K. Watanabe, T. Taniguchi, S. A. Maier, and K. S. Novoselov, "Sub-diffractional volume-confined polaritons in the natural hyperbolic material hexagonal boron nitride," Nat. Commun. **5**, 5221 (2014).
9. V. W. Brar, M. Seok Jang, M. Sherrott, S. Kim, J. J. Lopez, L. B. Kim, M. Choi, and H. Atwater, "Hybrid surface-phonon–plasmon polariton modes in graphene/monolayer h-BN heterostructures," Nano Lett. **14**, 3876–3880 (2014).

10. F. H. L. Koppens, D. E. Chang, and F. Javier García de Abajo, "Graphene plasmonics: a platform for strong light–matter interactions," Nano Lett. **11**, 3370–3377 (2011).
11. A. Vakil and N. Engheta, "Transformation optics using graphene," Science **332**, 1291–1294 (2011).
12. A. N. Grigorenko, M. Polini, and K. S. Novoselov, "Graphene plasmonics," Nat. Photonics **6**, 749–758 (2012).
13. T. Low and P. Avouris, "Graphene plasmonics for terahertz to mid-infrared applications," ACS Nano **8**, 1086–1101 (2014).
14. W. Zhu, I. D. Rukhlenko, L. Si, and M. Premaratne, "Graphene-enabled tunability of optical fishnet metamaterial," Appl. Phys. Lett. **102**, 121911 (2013).
15. W. Zhu, I. D. Rukhlenko, L. Si, and M. Premaratne, "Graphene metamaterial for optical reflection modulation," Appl. Phys. Lett. **102**, 241914 (2013).
16. I. D. Rukhlenko, A. Pannipitiya, M. Premaratne, and G. P. Agrawal, "Exact dispersion relation for nonlinear plasmonic waveguides," Phys. Rev. B. **84**, 113409 (2011).
17. D. R. Smith and D. Schurig, "Electromagnetic wave propagation in media with indefinite permittivity and permeability tensors," Phys. Rev. Lett. **90**, 077405 (2003).
18. A. J. Hoffman, L. V. Alekseyev, S. S. Howard, K. J. Franz, D. Wasserman, V. A. Podolskiy, E. E. Narimanov, D. L. Sivco, and C. Gmachl, "Negative refraction in semiconductor metamaterials," Nat. Mater. **6**, 946–950 (2007).
19. Z. Jacob, L. V. Alekseyev, and E. E. Narimanov, "Optical hyperlens: far-field imaging beyond the diffraction limit," Opt. Express **14**, 8247–8256 (2006).
20. C. L. Cortes, W. Newman, S. Molesky, and Z. Jacob, "Quantum nanophotonics using hyperbolic metamaterials," J. Opt. **14**, 063001 (2012).
21. A. Poddubny, I. Iorsh, P. Belov, and Y. Kivshar, "Hyperbolic metamaterials," Nat. Photonics **7**, 948–957 (2013).
22. L. Ferraria, C. Wub, D. Lepaged, X. Zhang, and Z. Liu, "Hyperbolic metamaterials and their applications," Prog. Quantum Electron. **40**, 1–40 (2015).
23. S. V. Zhukovsky, O. Kidwai, and J. E. Sipe, "Physical nature of volume plasmon polaritons in hyperbolic metamaterials," Opt. Express **21**, 14982–14987 (2013).
24. H. Hajian, A. Soltani-Vala, and M. Kalafi, "Characteristics of band structure and surface plasmons supported by a one-dimensional graphene–dielectric photonic crystal," Opt. Commun. **292**, 149–157 (2013).
25. L. A. Falkovsky, "Optical properties of graphene," J. Phys. Conf. Ser. **129**, 012004 (2008).
26. I. Iorsh, I. S. Mukhin, I. V. Shadrivov, P. A. Belov, and Y. S. Kivshar, "Hyperbolic metamaterials based on multilayer graphene structures," Phys. Rev. B **87**, 075416 (2013).
27. M. A. K. Othman, C. Guclu, and F. Capolino, "Graphene-based tunable hyperbolic metamaterials and enhanced near-field absorption," Opt. Express **21**, 7614–7632 (2013).
28. H. Hajian, H. Caglayan, and E. Ozbay, "Long-range Tamm surface plasmons supported by graphene–dielectric metamaterials," J. Appl. Phys. **121**, 033101 (2017).
29. Y. C. Chang, C. H. Liu, C. H. Liu, S. Zhang, S. R. Marder, E. E. Narimanov, Z. Zhong, and T. B. Norris, "Realization of mid-infrared graphene hyperbolic metamaterials," Nat. Commun. **7**, 10568 (2016).
30. J. D. Joannopoulos, S. G. Johnson, J. N. Winn, and R. D. Meade, *Photonic Crystals: Molding the Flow of Light*, 2nd Ed. (Princeton University, 2008).
31. E. E. Narimanov, "Photonic hypercrystals," Phys. Rev. X **4**, 041014 (2014).
32. W. S. Boyle, A. D. Brailsford, and J. K. Galt, "Dielectric anomalies and cyclotron absorption in the Infrared: observations on bismuth," Phys. Rev. **109**, 1396–1398 (1958).
33. T. Galfsky, Z. Sun, C. R. Considine, C. T. Chou, W. C. Ko, Y. H. Lee, E. E. Narimanov, and V. M. Menon, "Broadband enhancement of spontaneous emission in two-dimensional semiconductors using photonic hypercrystals," Nano Lett. **16**, 4940–4945 (2016).
34. A. Al Sayem, M. M. Rahman, M. R. C. Mahdy, I. Jahangir, and M. S. Rahman, "Negative refraction with superior transmission in graphene–hexagonal boron nitride (hBN) multilayer hyper crystal," Sci. Rep. **6**, 25442 (2015).
35. J. Wu, L. Jiang, J. Guo, X. Dai, Y. Xiang, and S. Wen, "Tunable perfect absorption at infrared frequencies by a graphene–hBN hyper crystal," Opt. Express **24**, 17103–17114 (2016).
36. H. Hajian, A. SoltaniVala, and M. Kalafi, "Effect of uniaxial anisotropy of left-handed layers on created surface waves in a one dimensional photonic crystal," Physica B **406**, 4094–4099 (2011).
37. H. Hajian, A. Soltani-Vala, and M. Kalafi, "Tunable far-IR bandgaps in a one-dimensional graphene–dielectric photonic crystal," Phys. Status Solidi C **9**, 2614–2617 (2012).
38. K. C. Huang, P. Bienstman, J. D. Joannopoulos, K. A. Nelson, and S. Fan, "Phonon-polariton excitations in photonic crystals," Phys. Rev. B **68**, 075209 (2003).
39. K. C. Huang, E. Lidorikis, X. Jiang, J. D. Joannopoulos, K. A. Nelson, P. Bienstman, and S. Fan, "Nature of lossy Bloch states in polaritonic photonic crystals," Phys. Rev. B **69**, 195111 (2004).
40. G. W. Hanson, "Quasi-transverse electromagnetic modes supported by a graphene parallelplate waveguide," J. Appl. Phys. **104**, 084314 (2008).
41. H. Hajian, A. Soltani-Vala, and M. Kalafi, "Optimizing terahertz surface plasmons of a monolayer graphene and a graphene parallel plate waveguide using one-dimensional photonic crystal," J. Appl. Phys. **114**, 033102 (2013).
42. D. Smirnova, P. Buslaev, I. Iorsh, I. V. Shadrivov, P. A. Belov, and Y. S. Kivshar, "Deeply subwavelength electromagnetic Tamm states in graphene metamaterials," Phys. Rev. B **89**, 245414 (2014).